POLITECNICO
MILANO 1863

SCUOLA DI INGEGNERIA INDUSTRIALE
E DELL'INFORMAZIONE

EXECUTIVE SUMMARY OF THE THESIS

Image-based finite element modelling of tricuspid valve biomechanics

TESI MAGISTRALE IN BIOMEDICAL ENGINEERING – INGEGNERIA BIOMEDICA

Author: Simona Vailetta

Advisor: Prof. Emiliano Votta

Co-advisor: Davide Tondi

Academic year: 2022-2023

1. Introduction

The tricuspid valve (TV) is the atrio-ventricular valve of the right heart. In physiological conditions, its complex structure ensures the unidirectional blood flow from the right atrium (RA) to the right ventricle (RV). The function of the TV can be affected by several diseases. In Western society, the most common one is tricuspid regurgitation (TR), which is secondary to left heart disease in 90% of cases. This condition affects about 1.6 million people in the USA alone [1]. For decades, TR has been considered a benign condition, hence TR pathophysiology and biomechanics have been poorly investigated. Recently, studies have shown that TR causes an increased risk of mortality, and this has attracted the interest of the scientific community. In this context, the development of finite element (FE) models to investigate the effects of pathologies and surgical treatments on TV biomechanics has gained interest, given their capability to quantify strains and stresses that would be difficult or impossible to measure experimentally, as well as the possibility to account for valve-specific morphology and kinematics as obtained from medical imaging.

On this basis, this study aims at defining a FE modelling strategy to quantify TV biomechanics from echocardiographic images. Starting from imaging of a porcine heart acquired on a test bench, the work focused on tackling three key aspects:

i) the modelling of chordae tendineae (CTs). CTs are not detectable with the main imaging technologies. Thus, different approaches to the modelling of CT topology, CT tissue stress-strain behaviour, and unloaded CT length were analysed, testing their effect on the capability of the FE model to reproduce the ground truth evidence from ultrasound data; ii) the definition of a complete modelling workflow suitable to reproduce pathological conditions; iii) the capability of the FE model to predict the effects of surgical interventions, with specific reference to the PM approximation strategy proposed by Jaworek et el. [2] to treat TR. Furthermore, the impact of the repair procedure on systolic TV biomechanics was assessed.

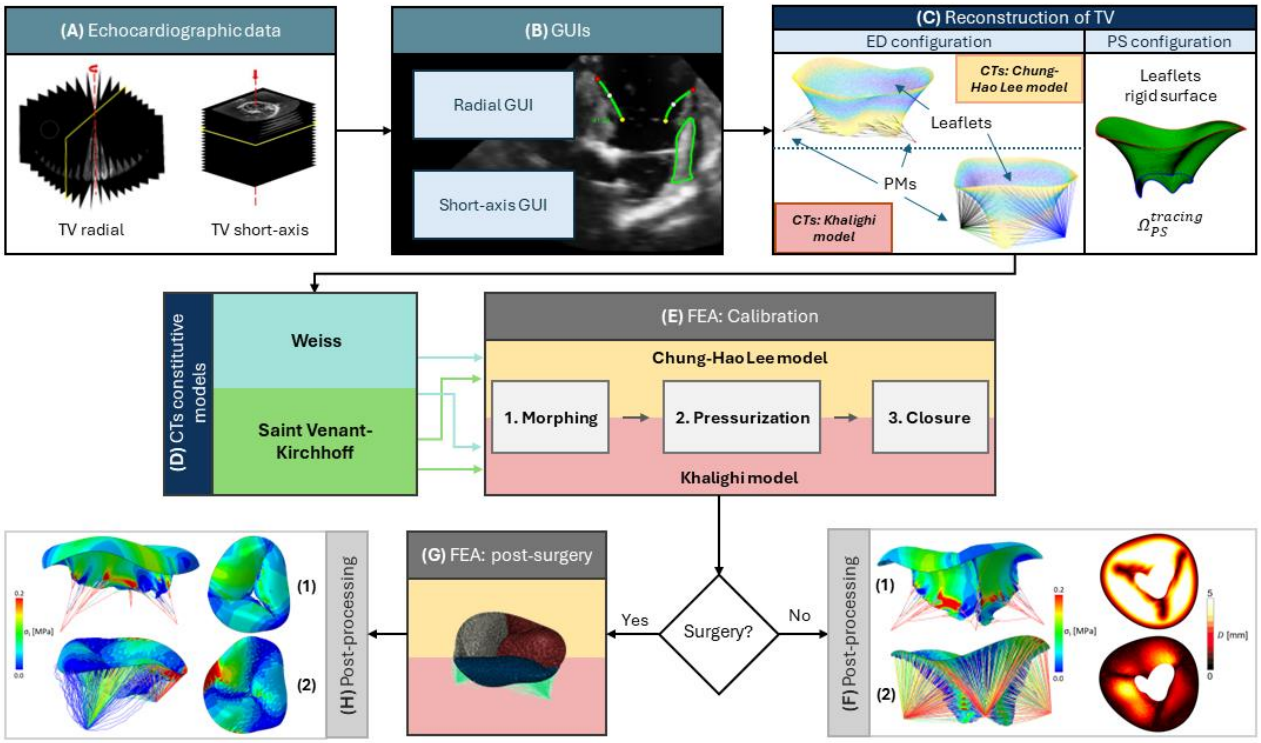

Figure 1: Overview of the project workflow

2. Methodology

The 3D echocardiographic data used for the present work were acquired on an explanted porcine heart using a test bench (mock circulatory loop system) during Locatelli and Manini's thesis [3]. Cartesian DICOM images were acquired with a Philips iE33 system with a TEE trans-oesophageal probe (CX7-2t, Philips, Eindhoven, The Netherlands). 30 frames/cycle Data with a 0.696x0.688x0.538 mm space-resolution were acquired in 30 frames/cardiac cycle. Data were acquired on a TV affected by functional regurgitation before and after PM approximation with a 60% reduction in the distance from the antero to the posterior PM. Pre-existing MATLAB scripts (Version R2023a, The MathWorks, Inc., Natick, MA, USA) were used to navigate the 3D ultrasound data, to set a cylindrical reference frame with the z-axis centred and orthogonal to the TV orifice, and to interpolate the 3D ultrasound data on 18 radial planes evenly rotated around the z-axis and 20 short-axis planes orthogonal to the z-axis with an inter-plane distance of 2 mm (Fig. 1.A).

2.1. GUIs Development

Two graphical user interfaces (GUIs) were implemented in MATLAB, which allowed to trace TV sub-structures (annulus, free margin (FRM), leaflets, papillary muscles (PMs) and commissures) in radial and short-axis planes, respectively (Fig. 1.B). An *ad hoc* viewer was integrated in the GUIs to allow for checking on the fly possible inaccuracies in the tracings.

2.2. TV FE model

In the pre-approximation images, the TV was traced at end-diastole (ED) to define the valve-specific initial configuration of the TV model, and at systolic peak (SP) to define the motion of the TV annulus between ED and SP, and the ground truth leaflet surface at SP. Tracings yielded the coordinates of the traced points in the 2D local reference frame of each image plane. These were automatically processed through the following steps:

1. transformation into the global 3D reference frame.
2. Identification of the centroid ($\mathbf{G}_{ann}$) and of the best fitting plane (π_{ann}) of the TV annulus points, which were used to define a cylindrical

reference frame with origin in $\mathbf{G}_{ann}$ and z-axis normal to π_{ann}.

3. Filtering and resampling of the 3D coordinates of the points of TV annulus and leaflets by means of 4th order fitting Fourier functions.

4. Triangulation of the resampled points to generate the TV leaflet surface. When reconstructed at SP, the surface was described as infinitely rigid ($\Omega_{SP}^{tracing}$) and used only as a auxiliary structure (Fig. 1.C). When reconstructed at ED, the surface was considered deformable and included in the TV FE model.

5. Identification of the commissures and thus of the anterior, posterior, and septal leaflets, based on a paradigmatic criterion.

6. Remeshing of the surface of the three leaflets at ED into 3-node triangular elements with characteristic size of 0.3 mm. The elements were assigned a space distribution of thickness values that ranged between minimum and maximum values reported by [4]

7. definition PM head position. As only two PMs were visible in the imaging, the third PM was defined based on geometrical criteria.

The discretized geometry of TV annulus and leaflets at ED diastole was complemented by the following features:

1. geometry of the CT apparatus, which was described through two approaches: the parametric model by Chung-Hao Lee et al. [5], which reflects a realistic distribution of branched CTs, and the functionally equivalent model by Khalighi et al. [6], which uses CTs uniformly distributed on the leaflets and requires an iterative tuning of CT length. The latter was originally designed to model the MV; it was appropriately adapted (Fig. 1.C) and tested with three values of chordal insertion density: 15±1, 20±1, 25±1 insertions/cm². In both cases, the CTs were modelled as truss elements with a constant cross section of 0.17 mm².

2. Mechanical properties of TV tissues. Leaflet tissue response was modelled using the Holzapfel constitutive model as in Locatelli and Manini thesis [3]. Two constitutive models were tested to render CT tissue response (Fig. 1.D). First, the Weiss model, where the stresses associated to the response of an isotropic matrix are superimposed to those associated to the presence of preferentially oriented fibres, which have the form:

$$\boldsymbol{S}_f = \lambda_f \frac{\partial W_f}{\partial \lambda_f} \hat{\boldsymbol{N}}_f \otimes \hat{\boldsymbol{N}}_f = \\ = \hat{\boldsymbol{N}}_f \otimes \hat{\boldsymbol{N}}_f \cdot \begin{cases} 0 & \boldsymbol{if} \quad \lambda_f < 1 \\ a_3 \left[e^{a_4 (\lambda_f - 1)} - 1 \right] & if \ 1 \leq \lambda_f \leq \lambda_f^* \\ a_5 \lambda_f + a_6 & if \ \lambda_f > \lambda_f^* \end{cases} \quad (\mathbf{2.1})$$

Where $\boldsymbol{S}_f$ is the second Piola-Kirchoff stress tensor associated to the fibres, $\hat{\boldsymbol{N}}_f$ is the unitary vector defining the initial local direction of the fibres, λ_f is the fibres' stretch ratio, λ_f^* is the stretch ratio causing the full recruitment of the fibres, and a_3, a_4, a_5, a_6 are the constitutive parameters.

Second, the Saint Venant-Kirchhoff model without the Poisson effect:

$$S_{ff} = (\lambda + 2\mu) E_{ff} \quad (\mathbf{2.2})$$

Where λ, μ are the Lamè constants, and S_{ff} and E_{ff} are the normal components of the second Piola-Kirchoff stress tensor and of the Cauchy-Green tensor in the fibre direction.

In the post-approximation images, the annulus and the PMs were traced again at ED and SP. Tracings were processed as already described.

2.3. Simulations

To evaluate which approach allowed for best reproducing TV closure as shown by echocardiographic imaging, two FE procedures were defined using the TV configuration at ED as initial and stress-free configuration: a one-step simulation and a three-simulation strategy (Fig.1.E). All simulations were performed with the commercial FE solver Abaqus/Explicit (SIMULIA, Dassault Systèmes).

One-step simulation: this type of simulation was only used for the model by Chung-Hao Lee et al. [5]. Consistently with previous studies on TV FE modelling [7], in a single step lasting 0.235 s TV closure was induced by loading the ventricular surface of the leaflets with an experimentally measured time-dependent pressure [3] while prescribing 3D displacements to the annular and PM nodes to reproduce their motion as reconstructed from tracings at ED and PS. Leaflet contact was modelled assuming penalty contact and a 0.01 friction coefficient.

Three-simulation strategy: this strategy was tested on four models corresponding to the possible combinations of the two CT topologies with the two CT constitutive models. Based on

Khalighi et al. [6], the following sequence of simulations was implemented (Fig. 1.E):

Morphing - PMs were initially set in their position at PS, CTs were assumed hyper-deformable and linear elastic ($E = 5kPa$, $\nu = 0.3$), and CONNECTOR elements were defined connecting some nodes on the FRM of the deformable ED leaflet surface to their counterpart on the FRM of $\Omega_{SP}^{tracing}$. A two-step simulation was run, wherein each step lasted 1 s: in the first step, annulus nodes were moved from their ED position to their SP position, while CONNECTOR elements were shortened to drive the FRM nodes on the FRM of $\Omega_{SP}^{tracing}$. In the second step, a pressure ramp from 0 to 5 mmHg loaded the ventricular surface of the leaflets while contact between the atrial side of the leaflet and $\Omega_{SP}^{tracing}$ was modelled. At the end of the simulation, the new coordinates (Ω_{SP}^{leaf}) of the leaflet nodes were extracted.

Pressurization: Ω_{SP}^{leaf} was used to calculate the length of the CTs at PS and hence derive their length at ED. This simulation assumed Ω_{SP}^{leaf} as initial configuration of the leaflets. CTs were described as hyper-rigid and linear elastic (E = 100GPa, ν = 0.475). In a single step lasting 1s, the ventricular surface of Ω_{SP}^{leaf} was loaded with the experimentally determined pressure load. At the end of the simulation, the reaction force (RF) for each CT was extracted and divided by its initial cross-sectional area to compute the first Piola-Kirchhoff CT stress. In the case of the Saint-Venant Kirchhoff constitutive model, the axial stretch ratio was obtained through the constitutive model (Algorithm 1).

Algorithm 1 Calculation of λ_{11} with Saint-Venant Kirchhoff model

1: $eqn = (\lambda + 2 * \mu) * \frac{1}{2} * (\lambda_{11}{}^2 - 1) * \lambda_{11} - P_{11} = 0$
2: % solution calculated with *vpasolve* function

For the Weiss model, an iterative algorithm was needed to establish the value of the fiber stretch ratio. Upon initialization of λ_{ff} to 1 and of λ_{ref}>>1, while the error ε between the λ_{ff} and λ_{ref} exceeds 0.005 the algorithm identifies which model branch to use and updates λ_{ff} (Algorithm 2).

For each CT, based on λ_{ff} and on the current length the initial length and the origin in the 3D space were obtained, with the condition that CTs should still pass through the corresponding PM.

In the case of Chung-Hao Lee's model, the change in length was only applied to the section between the PM and the main branch.

Algorithm 2 Iterative estimation of λ_{ff} for Weiss model

1: **While** $(\lambda_{ref} - \lambda_{ff}) > \varepsilon$
2: $\lambda_{ref} = \lambda_{ff}$;
3: **If** $\lambda_{ff} < \lambda_f^*$ % λ_f^* is the transition value
4: $eqn = 2 * \left(a_1 * \left(\lambda^2 - \left(\frac{1}{\lambda}\right)\right) - a_2 * \left(\left(\frac{1}{\lambda}\right)\right)^2 - \lambda\right) + +a_3 * \left(e^{a_4 * (\lambda - 1) - 1}\right) - t_{ff} = 0$
5: % solution calculated with *vpasolve* function yielding λ_{ff} based on t_{11} initialized out of the loop
6: **else**
7: $eqn = 2 * \left(a_1 * \left(\lambda^2 - \left(\frac{1}{\lambda}\right)\right) - a_2 * \left(\left(\frac{1}{\lambda}\right)\right)^2 - \lambda\right) + +a_5 * \lambda + a_6 - t_{ff} = 0$
8: % solution calculated with *vpasolve* function yielding λ_{ff} based on t_{11} initialized out of the loop
9: **end**
10: $t_{ff} = P11 * \lambda_{ff}$;
11: **end**
12: $l_0 = l_{end} * \lambda_{ff}$

Closure: the TV was initially in its configuration at ED, with CTs originating at the points identified by the *Pressurization* simulation. In the first step lasting 1s, the origin of the CTs was shifted to the position of the corresponding PM at ED. In the second step, lasting 0.235 s, annulus and PM nodes were moved from their position at ED to their position at SP, while the ventricular surface of the leaflets was loaded with the experimentally measured physiological pressure.

Post-surgery simulation: starting from the configurations obtained at the end of the *Pressurization* simulation, a two-step simulation was performed. In the first step, lasting 1 s, the annulus points and CT origins were moved to the post-surgery ED position of the annulus and of the PMs, respectively. In the second step, lasting 0.235 s, TV closure was simulated: the experimentally measured pressure was applied on the ventricular side of the leaflets, and the annulus and PMs were shifted from the post-surgery ED position to the post-surgery PS position (Fig. 1.G).

3. Results

3.1. Pre-approximation TV closure

At the end of the *Closure* simulation, the reliability of the obtained configuration was analysed to identify the best CT model in terms of topology and constitutive model. For each model variant, the Euclidean distance between $\Omega_{PS}^{tracing}$ and Ω_{SP}^{leaf} was computed nodewise and described as median (25th percentile ÷ 75th percentile).

When CTs were described through the Chung-Hao Lee approach with fine-tuning of the CT initial length, the lowest Euclidian distance, i.e., 2.59 (1.14 ÷ 4.42), was obtained when CT mechanical properties were described through the De Saint Venant-Kirchhoff model; in that case, the regurgitant area was 13.24 % of the orifice area. Of note, leaflet surface at PS tended to bulge into the atrium, due to the absence of CTs inserted in the leaflet belly, consistently with [7].

When the Khalighi approach was used, the lowest values, i.e., 1.11 (0.46 ÷ 1.91)mm were obtained for a chordal density of 25±1 insertions/cm². The regurgitation area characterizing Ω_{SP}^{leaf} was 12.63% of the orifice area, which well agreed with the corresponding datum, i.e., 12.23%, obtained on $\Omega_{PS}^{tracing}$.

The two approaches yielded different results in terms of leaflet max principal stresses (from here on, simply stresses) at PS when simulating the pre-approximation TV closure.

When the Chung-Hao Lee approach with chordae length fine tuning was used, leaflet stresses were not affected by the constitutive model chosen to describe CT mechanical properties. Leaflet stresses has a median value of 0.06 MPa and interquartile range of 0.04 ÷ 0.09 MPa. However, stress hot-spots at the chordal insertions were detected. (Fig. 1.F1) CT stresses instead were affected by the adopted CT constitutive model: their median value was 0.40 and 0.63 MPa when using the Weiss and the De Saint Venant-Kirchhoff model, respectively.

When the Khalighi approach was used, and in particular for a CT insertion density of 25±1 insertions/cm², leaflet stresses had a median value of 0.03 MPa and an interquartile range 0.01 ÷ 0.07 MPa, while CT stresses had a median value of 0.14 MPa and an interquartile range of 0.09 ÷ 0.21 MPa (Fig. 1.F2).

3.2 Post-approximation TV closure

In post-approximation simulations, the the Khalighi approach and the Chung-Hao Lee approach with CT initial length tuning both captured well the regurgitant area at PS, which was dramatically reduced as compared to the pre-approximation case. Yet, they yielded very different results on any other aspect.

Even qualitatively, the leaflet configuration at PS computed by the two approaches was very different, the former approach yielding a very asymmetrical configuration with a hyper-tethered leaflet and two bulging leaflets. Instead, the Chung-Hao Lee approach computed a configuration with an almost three-leaflet symmetry (Fig. 1.H2).

Therefore, evident differences were detected in terms of leaflet stresses. When the Khalighi approach was used, no matter what CT insertion density or what CT constitutive model were adopted, stresses were characterized by a median value of about 0.025 MPa, with interquartile range 0.008 ÷ 0.048 MPa and stress peaks up to 0.16 MPa localized at CT insertions on the hyper-tethered leaflet. When the Chung-Hao Lee approach with chordae length fine tuning was used , leaflet stresses hada medial value of 0.05 MPa, an interquartile range 0.03 ÷ 0.07 MPa, with peak stresses up to 0.17 and 0.21 MPa depending on the adopted CT constitutive model (Fig. 1.H1).

4. Discussion

During the thesis work, the available ultrasound data revealed issues in terms of quality and compatibility of proportions when comparing data from different valves, but also data from the same valve pre- and post-surgery. Furthermore, the preparation of the data for required the use of tools that was not completely developed for this purpose. The workflow should be applied again using images acquired using a well-defined and repeatable protocol. In the future, the work could be transferred to the analysis of in vivo images. The Matlab scripts devoted to 3D data navigation and processing could be optimized, and this optimization process could benefit from the standardization of the acquisition protocol.

Manual image segmentation relies heavily on the operator's experience and skill. In the future, one could evaluate the implementation of software

capable of performing an automatic or semi-automatic segmentation of images, perhaps based on artificial intelligence.

The reconstruction and simulation phases required a careful study of the anatomy and the current state of the art of FE models. The modelling of the CTs emerged as a critical point of FE simulations. For this reason, it was decided in the present work to investigate in detail the impact of the geometric and material characterisation of CTs.

The results showed that, no matter the specific approach adopted, the initial tuning of chordae length allows for better capturing the TV configuration at PS. Yet, when the Chung-Hao Lee approach is used the calibration applied only to the initial section, from the PM to the first branching, is simplistic; the calculation of the new length should apply to all branching levels.

The functionally equivalent model with a chordal density of 25±1 insertions/cm² and described with the Weiss constitutive model is the one that obtained the best morphological characterisation. In addition, the associated stresses and deformations are distributed in a manner consistent with the application of pressure. However, the same model does not perform adequately when displacements are applied between the structures on which the calibration was performed, as in the case of PM approximation. This limitation suggests that the capability to replicate ground truth evidence is not necessarily matched by the capability to predict TV biomechanics other scenarios.

Chung-Hao Lee's model, on the other hand, allows the analysis of post-surgery valve biomechanics. The Weiss model turns out to be the most formally correct as it allows a correct description of the recruitment of collagen fibres during the simulation of valve closure.

The results of the post-approximation simulations suggest that PM approximation may not overstress TV leaflets when used to treat TR: stress peaks are not greater than those computed in the pre-approximation simulations.

The main limit of this work was the application of the workflow to echocardiographic images of a single TV. To assess the repeatability of the workflow, a larger amount of data would have to be applied and it would be interesting to translate it to clinical images from patients.

Despite this, the results obtained from the two models for defining the geometry of CTs applied to the case of the pathological and post-surgery valve are particularly interesting. The implementation of a mixed model that exploits the strengths and solves the main issues of the two models could be considered. The patient-specific description of CTs is not allowed as the information from imaging is limited. The functional equivalent model completely solves this problem. Of interest in Chung-Hao Lee's model is the positioning of the chordal insertions consistent with the anatomical characterisation of the CTs. A functionally equivalent model could be considered, but with unevenly distributed chordal insertions. A higher density could be defined in the rough zone to stabilise the TV, but a reduction of density might be applied to the clear and basal zone of the valve. This should allow to obtain a model that correctly describes the biomechanical characteristics of the TV with TR, on which the calibration of the CTs is performed, and limit artefacts in the post-surgery simulation.

References

[1] E. Yucel, P. B. Bertrand, J. L. Churchill, and M. Namasivayam, "The tricuspid valve in review: Anatomy, pathophysiology and echocardiographic assessment with focus on functional tricuspid regurgitation," *J. Thorac. Dis.*, vol. 12, no. 5, pp. 2945–2954, 2020, doi: 10.21037/jtd.2020.02.42.

[2] M. Jaworek *et al.*, "Treatment of Tricuspid Regurgitation at Subvalvular Level: Hemodynamic and Morphological Assessment in Ex-Vivo Beating Heart Model," *Struct. Hear.*, vol. 4, no. 1, pp. 36–45, 2020, doi: 10.1080/24748706.2019.1686555.

[3] C. M. G. Locatelli, "Tricuspid Valve Finite Element Modeling based on 3D Ultrasound Imaging: Development of an Improved Method and Application to the Study of Papillary Muscle Approximation as a mean to treat Functional Tricuspid Regurgitation," 2018.

[4] S. Heyden *et al.*, "Material modeling of cardiac valve tissue: Experiments, constitutive analysis and numerical investigation," *J. Biomech.*, vol. 48, no. 16, pp. 4287–4296, 2015, doi: 10.1016/j.jbiomech.2015.10.043.

[5] C. Lee *et al.*, *Mechanics of the Tricuspid Valve — From Clinical Diagnosis / Treatment , In-*

Vivo and In-Vitro Investigations , to Patient-Specific Biomechanical Modeling. 2019.

[6] A. H. Khalighi, B. V. Rego, A. Drach, R. C. Gorman, J. H. Gorman, and M. S. Sacks, "Development of a Functionally Equivalent Model of the Mitral Valve Chordae Tendineae Through Topology Optimization," *Ann. Biomed. Eng.*, vol. 47, no. 1, pp. 60–74, 2019, doi: 10.1007/s10439-018-02122-y.

[7] D. W. Laurence, E. L. Johnson, M. Hsu, R. Baumwart, and A. Mir, "A pilot in-silico modeling-based study of the pathological effects on the biomechanical function of tricuspid valves Devin," *Heal. Res. Alliance*, vol. 33, no. 8, pp. 1089–1091, 2020, doi: 10.1007/BF01945988.